Journal of Virology®

PATHOGENESIS AND IMMUNITY

Mouse Scarb2 Modulates EV-A71 Pathogenicity in Neonatal Mice

Wakako Miwatashi,[a] Minori Ishida,[a] Ayako Takashino,[a] Kyousuke Kobayashi,[a] Midori Yamaguchi,[b] Hiroshi Shitara,[b] Satoshi Koike[a]

[a]Neurovirology Project, Department of Disease and Infection, Tokyo Metropolitan Institute of Medical Science, Tokyo, Japan
[b]Laboratory for Transgenic Technology, Center for Basic Technology Research, Tokyo Metropolitan Institute of Medical Science, Tokyo, Japan

Wakako Miwatashi and Minori Ishida contributed equally to this article. Author order was determined because Wakako Miwatashi joined this project earlier.

ABSTRACT Enterovirus A71 (EV-A71) is a human pathogen that causes hand, foot, and mouth disease, which can progress to severe neurological disease. EV-A71 infects humans via the human scavenger receptor B2 (hSCARB2). It can also infect neonatal mice experimentally. Wild-type (WT) EV-A71 strains replicate primarily in the muscle of neonatal mice; however, susceptibility lasts only for a week after birth. Mouse-adapted (MA) strains, which can be obtained by serial passages in neonatal mice, are capable of infecting both muscle and neurons of the central nervous system. It is not clear how the host range and tropism of EV-A71 are regulated and why neonatal mice lose their susceptibility during development. We hypothesized that EV-A71 infection in neonatal mice is mediated by mouse Scarb2 (mScarb2) protein. Rhabdomyosarcoma (RD) cells expressing mScarb2 were prepared. Both WT and MA strains infected mScarb2-expressing cells, but the infection efficiency of the WT strain was much lower than that of the MA strain. Infection by WT and MA strains *in vivo* was abolished completely in *Scarb2*$^{-/-}$ mice. *Scarb2*$^{+/-}$ mice, in which Scarb2 expression was approximately half of that in *Scarb2*$^{+/+}$ mice, showed a milder pathology than *Scarb2*$^{+/+}$ mice after infection with the WT strain. The Scarb2 expression level in muscle decreased with aging, which was consistent with the reduced susceptibility of aged mice to infection. These results indicated that EV-A71 infection is mediated by mScarb2 and that the severity of the disease, the spread of virus, and the susceptibility period are modulated by mScarb2 expression.

IMPORTANCE EV-A71 infects humans naturally but can also infect neonatal mice. The tissue tropism and severity of EV-A71 disease are determined by several factors, among which the virus receptor is thought to be important. We show that EV-A71 can infect neonatal mice using mScarb2. However, the infection efficiency of WT strains via mScarb2 is so low that an elevated virus-receptor interaction associated with mouse adaptation mutation and decrease in mScarb2 expression level during development modulate the severity of the disease, the spread of virus, and the susceptibility period in the artificial neonatal mice model.

KEYWORDS EV-A71, neonatal mouse model, Scarb2, mouse adaptation

Enterovirus A71 (EV-A71) belongs to species A of the genus *Enterovirus* (EV-A) in the family *Picornaviridae*. EV-A71 has an icosahedral capsid consisting of 60 copies of each of four capsid proteins, namely, VP1, VP2, VP3, and VP4, and a positive-sense, single-stranded RNA genome of approximately 7,400 bases (1, 2). EV-A71 is a causative agent of hand, foot, and mouth disease (HFMD), along with other members of EV-A. HFMD is generally a mild and self-limiting disease; however, the HFMD caused by EV-A71 is associated with severe neurological complications, such as aseptic meningitis, acute encephalitis, acute flaccid paralysis, and neurogenic pulmonary edema (3–5).

Editor Colin R. Parrish, Cornell University

Address correspondence to Satoshi Koike, koike-st@igakuken.or.jp.
The authors declare no conflict of interest.

Received 5 April 2022
Accepted 29 June 2022
Published 14 July 2022

Outbreaks with many severe cases and even deaths have occurred repeatedly in Asia-Pacific regions (6). Therefore, EV-A71 infection is a serious public health concern.

The natural host of EV-A71 is humans. Transmission of EV-A71 in humans is primarily via the fecal-oral route. Initial viral replication occurs in the epithelial cells in the gastrointestinal tract (7). The virus then spreads through the body, and HFMD occurs as a result of replication of the virus in the skin (8). In most cases, the patients recover and the virus is cleared. However, infrequently, the virus enters the central nervous system (CNS) through an unknown mechanism(s). Neurons in the CNS are the sites of viral replication. Severe lesions occur in the CNS of fatal cases but not in other organs (7).

Human rhabdomyosarcoma (RD) cells but not mouse L929 cells are susceptible to EV-A71. The human scavenger receptor class B member 2 (hSCARB2) was identified as the essential receptor using this species-specific infection of EV-A71 (9). L929 cells transfected with the human *SCARB2* gene or cDNA showed full susceptibility to infection (9–11). SCARB2 also plays an important role in EV-A71 infection *in vivo*. In fatal human cases, SCARB2 expression is detected in EV-A71 antigen-positive cells, such as squamous epithelial cells of palatine tonsil and neurons in the CNS (7). Transgenic (tg) expression of hSCARB2 in mice permits the replication of EV-A71 in the CNS of adult mice, which are normally insusceptible, suggesting that hSCARB2 expression is required for EV-A71 infection *in vivo* (12). The virus binding site in hSCARB2 was investigated using chimeras of hSCARB2 and mScarb2. This investigation revealed that a region encoded in exon 4 of the *SCARB2* gene is necessary for the establishment of efficient infection (13). The amino acid identity of hSCARB2 and mScarb2 in this region is 76.2%, while that of the whole is 85.8%. Subsequently, a more precise structure of the virus-receptor complex was revealed by cryo-electron microscopy (14). The α-helices 4 and 5 in the apical region of the SCARB2 form the binding site on the receptor side, and the EF loop of VP2 and GH loop of the VP1 capsid proteins form the binding sites on the viral side. These results suggested that the interaction between EV-A71 and SCARB2 receptor plays an important role in determining host range.

Neonatal mice are susceptible to EV-A71 and other EV-A viruses (2) and have been used widely as an animal model because they are easy to handle; however, after EV-A71 infection, they do not exhibit the same pathological features as humans (15). First, the tissue tropism of EV-A71 in neonatal mice is different from that of humans. Neonatal mice show paralysis when the virus is inoculated intraperitoneally or subcutaneously. The main viral replication site of the virus is the skeletal muscle, as observed for other EV-As (2). This muscle-tropic infection is not observed in humans. Viral replication is observed in neurons in the CNS of neonatal mice but to a lesser extent than that in muscles. Second, the susceptibility of neonatal mice to infection is lost with increasing age. Neonatal mice up to 1 week old are susceptible to EV-A71, but after that, they lose susceptibility, and EV-A71 infection does not occur in adult mice. In humans, HFMD patients are mainly children younger than 5 years old. Infection in adults occurs, but it is rare because adults acquire immunity to EV-A71 through natural infection in childhood and do not develop the disease thereafter. Third, artificial adaptation of the virus to mice can increase its pathogenicity. Mouse-adapted (MA) strains have been obtained by passaging the virus several times in neonatal mice or rodent cells (15–17). The adaptation can extend the window of susceptibility to 2 weeks after birth and result in more extensive replication of the virus in the CNS. Many MA strains have a common mutation of lysine (K) to isoleucine (I) or methionine (M) at amino acid 149 of capsid protein VP2 (VP2-149) (17–20). Thus, MA mutations make the susceptibility period longer and the tissue tropism wider. In addition, AG129 mice (21), which are deficient in functional interferon α/β (IFN-α/β) and IFN-γ responses, show increased susceptibility (22). In combination with MA strains and AG129 mice, susceptibility has been shown to persist up to 10 weeks of age (23).

For a better understanding of *in vivo* EV-A71 infection at the molecular level, identification of the virus receptor and elucidation of the virus-receptor interaction are

necessary. Since amino acid VP2-149 is in the EF loop of VP2 that binds hSCARB2 (14), it was speculated that a K-to-I or a K-to-M mutation at VP2-149 would strengthen the interaction between mutant viruses and mScarb2. A mouse L929 cell-adapted virus was isolated after multiple passages in L929 cells, and L929 cells deficient in *Scarb2* gene function were generated using the CRISPR-Cas9 system. *Scarb2*-deficient L929 cells were not susceptible to the L929-adapted strain, suggesting that mScarb2 can serve as a receptor for this strain *in vitro* (24). This result also suggested strongly that MA strains may infect neonatal mice *in vivo* using mScarb2 as their receptor; thus, we decided to examine the possibility that mScarb2 would also act as a receptor for WT strains under certain circumstances, albeit with lower efficiency. To this end, we investigated the role of mScarb2 in cultured cells and neonatal mouse infection. Here, we present data showing that WT EV-A71 can infect mScarb2-expressing cells but with reduced efficiency and that the susceptibility of neonatal muscle and neurons to both WT and MA strains of EV-A71 is completely lost in *Scarb2*$^{-/-}$ mice. Taken together, the results suggest that the infection efficiency of WT EV-A71 is borderline for the establishment of infection and that slight changes in the virus-receptor interaction and/or mScarb2 expression level greatly modulate the pathogenicity of EV-A71 in neonatal mice.

RESULTS

Both wild-type and mouse-adapted strains of EV-A71 use mouse Scarb2 as their receptor with different efficiencies *in vitro*. We previously produced RD-ΔSCARB2 cells, which lack a functional *SCARB2* gene and are completely resistant to EV-A71 infection (25). To determine whether mScarb2 can serve as a receptor, either hSCARB2 or mScarb2 cDNA was expressed in RD-ΔSCARB2 cells using retrovirus vectors, producing RD-ΔSCARB2+hSCARB2-F and RD-ΔSCARB2+mScarb2-F, respectively. For simplicity, these cell lines are referred to as RDΔS2, RD+hS2, and RD+mS2, respectively (Fig. 1A). Human RD cells are highly permissive for enterovirus replication. It is therefore possible to evaluate the function of hSCARB2 and mScarb2 as receptors in the same human RD cell background. The ectopic expression of FLAG-tagged hSCARB2 and mScarb2 proteins was demonstrated by Western blotting using an anti-hSCARB2 antibody or an anti-FLAG antibody in RD+hS2 and RD+mS2 cells, respectively (Fig. 1B). Flow cytometry analysis of nonpermeabilized cells with the anti-hSCARB2 antibody revealed that at least some of the ectopically expressed receptor protein was present at the cell surface (Fig. 1C).

We prepared a representative of a wild-type (WT) and an MA strain using the SI/Isehara/Japan/99 strain (12). The amino acid residue at VP2-149 is K in WT and I in MA strains (referred to as VP2-149K and VP2-149I, respectively). We infected RD+hS2 and RD+mS2 cells with VP2-149K or VP2-149I strains and compared the plaque formation of the infected cells (Fig. 2A). The VP2-149K strain produced clear plaques on RD+hS2 cells but smaller numbers of turbid plaques on RD+mS2 cells. The VP2-149I strain produced clear plaques on both cell types. We then determined viral RNA copy number by reverse transcriptase quantitative PCR (RT-qPCR) and calculated the infection efficiency, defined as the number of plaques per RNA genome copy number (PFU/RNA copy) (Fig. 2B). The VP2-149K strain infected RD+hS2 cells with high efficiency ($10^{-2.37}$ PFU/RNA copy) and RD+mS2 with approximately 60 times lower efficiency ($10^{-4.12}$ PFU/RNA copy). The VP2-149I strain infected both cells with high efficiency, with $10^{-2.17}$ PFU/RNA copy in RD+hS2 cells and a slightly lower $10^{-2.84}$ PFU/RNA copy in RD+mS2 cells. Similarly, other EV-A71 WT (VP2-149K) strains, including N772-Sendai-2003, 2716-Yamagata-03, and Y90-3896 (26), produced turbid plaques on RD+mS2 cells and their infection efficiencies on RD+mS2 cells were 53- to 133-fold lower than that in RD+hS2 cells (data not shown). These results indicated that both WT (VP2-149K) and MA (VP2-149I) strains can infect via mScarb2 but the infection efficiency of WT strains via mScarb2 is much lower than that via hSCARB2.

Replication kinetics of the two strains in the two cell types were compared (Fig. 2C). RD+hS2 or RD+mS2 cells (10^6 cells) were infected with VP2-149K or VP2-149I (10^3 PFU

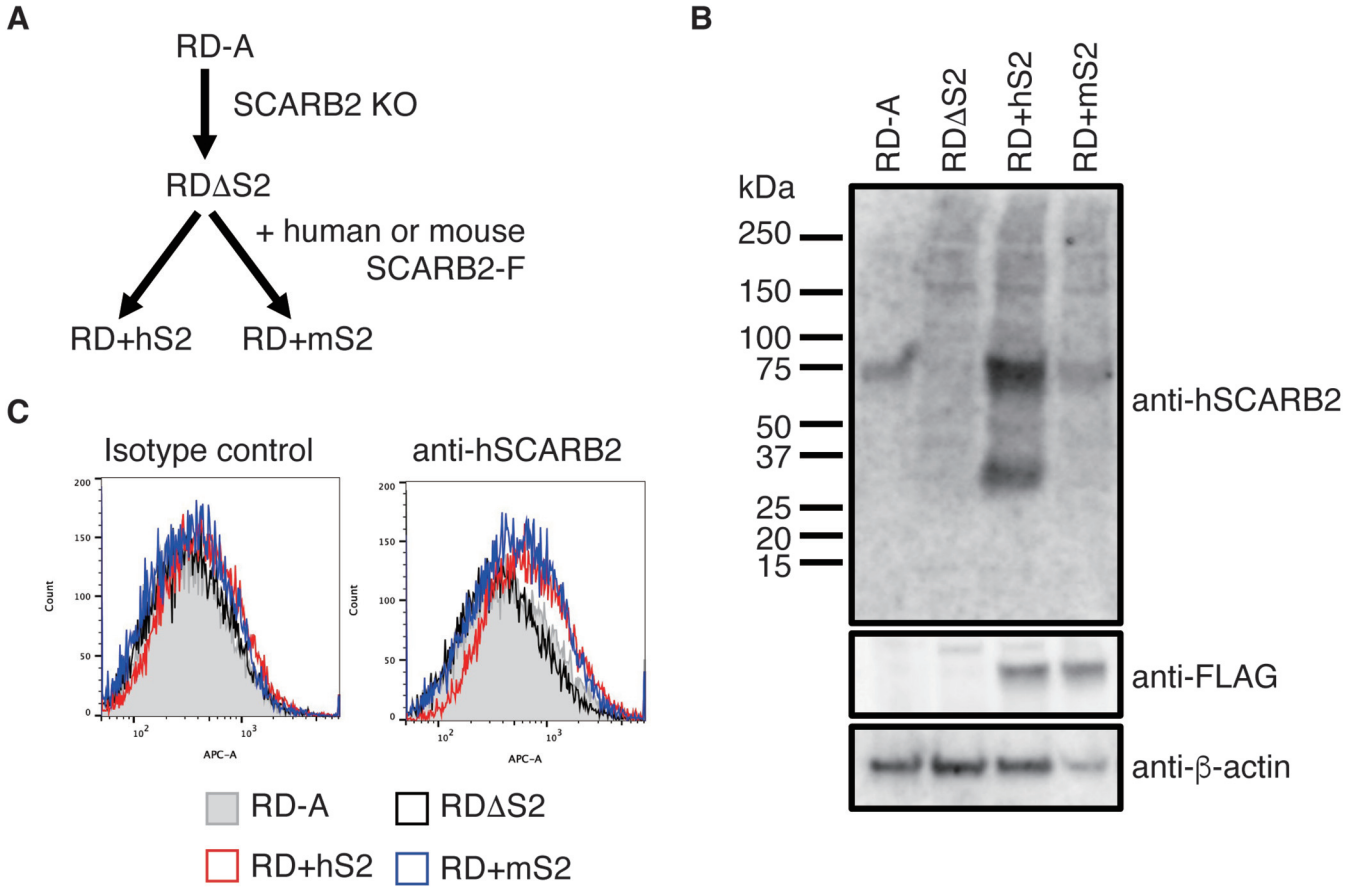

FIG 1 Preparation of RD cells expressing hSCARB2 or mScarb2. (A) hSCARB2 or mScarb2 cDNA was expressed in RDΔS2 cells, in which the endogenous h*SCARB2* gene was disrupted, using a retrovirus vector. (B) Expression of SCARB2 protein in RD+hS2 and RD+mS2 cells was detected by Western blotting using the anti-hSCARB2 antibody (top) or anti-FLAG antibody (middle). Bottom: The anti-β-actin antibody as a control. (C) FACS analysis of the SCARB2 protein using an anti-hSCARB2 antibody. Nonpermeabilized cells were stained with anti-hSCARB2 antibody and analyzed.

determined on RD+hS2 cells), and virus titer was monitored every 24 h for 5 days. As expected, the VP2-149K and VP2-149I strains grew at similar rates in RD+hS2 cells. The VP2-149I strain grew in the RD+mS2 cells, but the growth kinetics were retarded slightly. The VP2-149K strain had more retarded growth kinetics in the RD+mS2 cells and the maximum viral yield was more than 10 times lower than those of other cell-virus combinations. These results indicate that WT EV-A71 (VP2-149K) can infect via the mScarb2 but that its replication is inefficient.

Preparation of *mScarb2* knockout mice. We produced *Scarb2* knockout mice using the CRISPR-Cas9 system to determine whether EV-A71 infection in neonatal mice is mediated by mScarb2 *in vivo*. We obtained three different knockout lines and used line number 27 for further experiments. The number 27 knockout allele has a 2-nucleotide deletion in exon 4. The amino acids at positions 165 to 182 were altered and followed by a stop codon, resulting in the absence of a functional Scarb2 protein (Fig. 3A). The WT and knockout alleles can be discriminated by allele-specific PCR (Fig. 3B and C). Western blotting using an anti-mScarb2 antibody showed that the mScarb2 protein was absent from the embryonic fibroblasts derived from *Scarb2*$^{-/-}$ mice and that the Scarb2 protein level in *Scarb2*$^{+/-}$ was approximately half of that in *Scarb2*$^{+/+}$ mice. (Fig. 3D and E). The expression level of the *Scarb2* gene located on autosomes (chromosome 5) should be dependent on gene dosage. Thus, these results demonstrated that the *Scarb2* gene had been disrupted correctly. Immunohistochemical staining of the mScarb2 protein using the anti-mScarb2 antibody showed that Scarb2 is expressed widely in all organs, including the muscle and the CNS of *Scarb2*$^{+/+}$ neonatal mice (Fig. 3F and

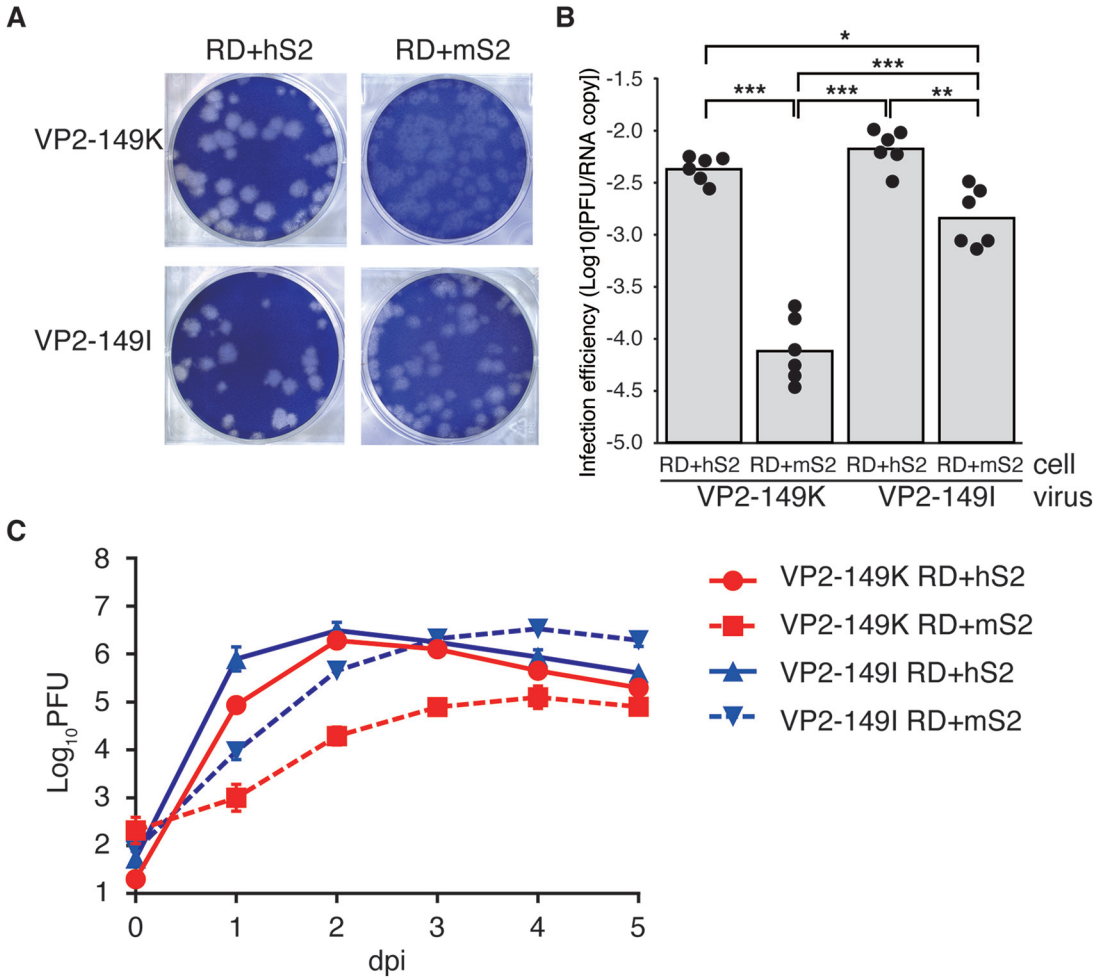

FIG 2 Plaque morphology and infection efficiency of VP2-149K and VP2-149I strains in RD+hS2 and RD+mS2 cells. (A) The plaques of VP2-149K and VP2-149I strains on RD+hS2 and RD+mS2 cells. Note that the plaques of the VP2-149K strain on RD+mS2 cells are turbid. (B) Infection efficiency of the two strains on the two cell types. The copy number of the virus was measured using RT-qPCR. The number of plaques was divided by the copy number. The experiments were repeated six times, and the mean value is shown. The statistical significance of each value was determined by Student's *t* test and corrected by the Bonferroni method. *, $P < 0.05$; **, $P < 0.01$; ***, $P < 0.001$. (C) Growth kinetics of VP2-149K and VP2-149I strains in the two cell types. Red and blue lines indicate the growth curve of the VP2-149K and VP2-149I strains, respectively. The solid lines and dotted lines indicate those in RD+hS2 and RD+mS2 cells, respectively. The titer was determined three times and the mean value ± standard deviation is shown. dpi, days postinfection.

H). The expression profile of mScarb2 was the same as that of hSCARB2 in humans and hSCARB2 in hSCARB2 tg mice, as reported previously (12). High levels of Scarb2 expression were observed in neurons of the CNS and in skeletal muscle, lung pneumocytes, intestinal epithelium, hepatocytes, renal tubular epithelium, and splenic germinal centers (data not shown). Expression of Scarb2 was not observed in *Scarb2*$^{-/-}$ mice (Fig. 3G and I). These results show that mScarb2 is expressed widely in WT mice but was absent from the knockout mice.

Knockout of mouse *Scarb2* gene abolished infection of both VP2-149K and VP2-149I viruses *in vivo*. We mated heterozygous *Scarb2*$^{+/-}$ mice and obtained progenies having all three possible genotypes. We infected the neonatal mice intraperitoneally with either the EV-A71 VP2-149K or the VP2-149I strain (1.7×10^5 50% tissue culture infective dose [$TCID_{50}$]) within 3 days after birth and recorded mortality. The CVA6 1421-Yamagata-2013 strain (27) was used as a control whose infection is not affected by the *Scarb2* genotype. CAV6 also belongs to EV-A and causes HFMD or herpangina in young children and infants. EV-A members CVA2, 3, 4, 5, 6, 10, and 12 use Kremen1 receptors to infect skeletal muscle and kill neonatal mice. The lethal infection is abolished in neonatal *Kremen1*$^{-/-}$ mice (28). A total of 43, 41, and 33 neonatal mice

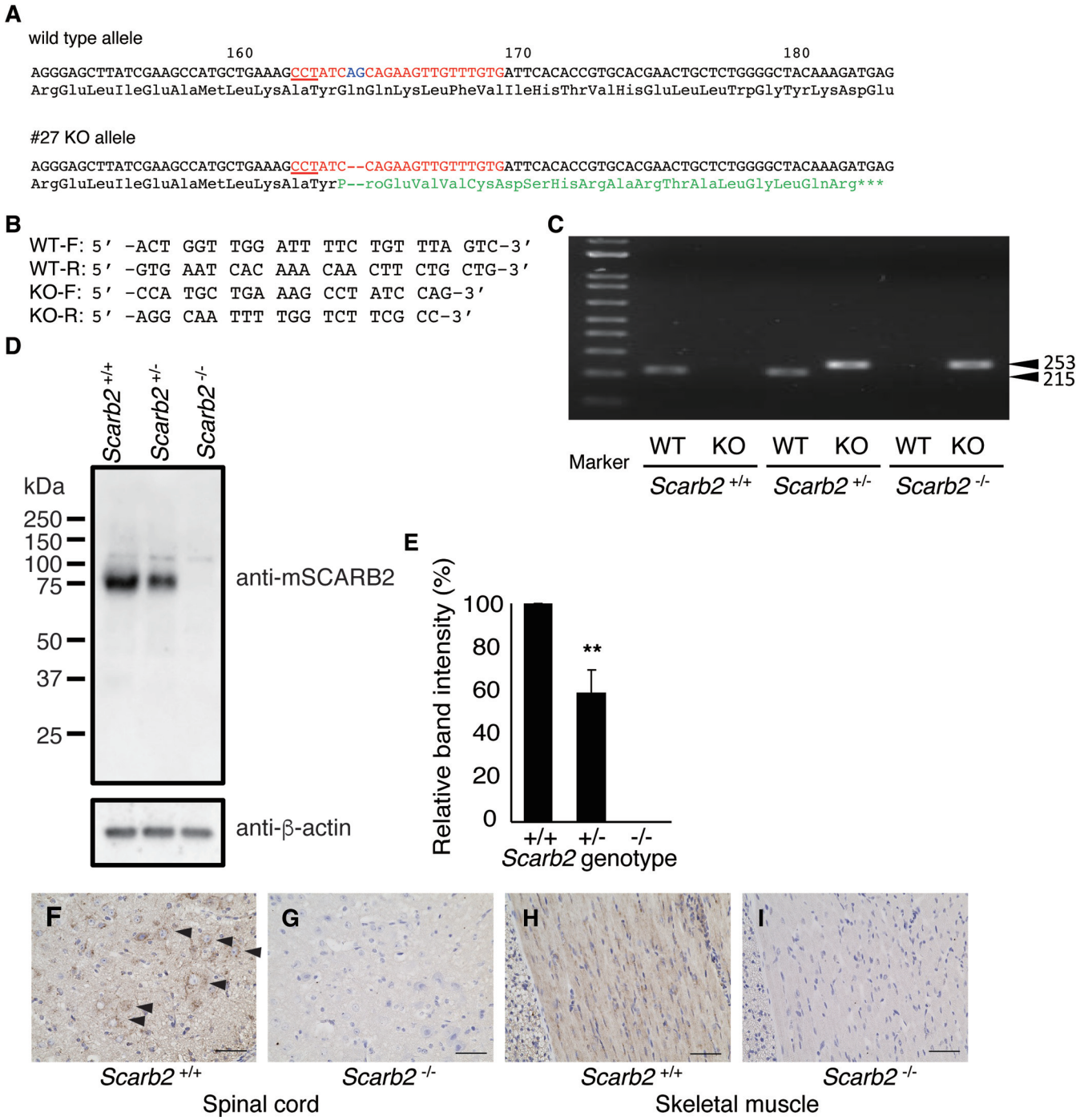

FIG 3 Generation of *Scarb2* knockout mice. (A) The WT and knockout alleles of the m*Scarb2* gene. Partial nucleotide (top line) and amino acid (bottom line) sequences of the exon 4 region are shown. The red letters indicate the position of sgRNA. The underline indicates the position of the PAM sequence. The blue letters indicate the position of two nucleotides deleted in the knockout allele. The green letters indicate the 17 amino acids altered by the 2-nucleotide deletion followed by the stop codon (asterisks). (B) Nucleotide sequences of the primers used for the WT and the knockout allele-specific PCR. (C) Allele-specific PCR. The DNA of the pups was subjected to allele-specific PCR, and the PCR products of 253 and 215 bp were observed for WT and knockout alleles, respectively. (D) Detection of mScarb2 protein. Fibroblasts were prepared from the embryos of each genotype and 200 ng of protein was loaded per lane. The Scarb2 protein was detected by Western blotting using anti-mScarb2 (top). Note that the Scarb2 protein was not detected in $Scarb2^{-/-}$ MEFs. The same membrane was reprobed by anti-β actin antibody as a control (bottom). (E) Comparison of mScarb2 expression levels. The Scarb2 expression level was normalized by the β-actin level and that of $Scarb2^{+/+}$ was set as 100%. The experiments were repeated three times and the mean value ± standard deviation is shown. The statistical significance of the difference in values for each condition, using $Scarb2^{+/+}$ as the standard, was determined by Student's *t* test. **, $P < 0.01$. (F to I) Immunohistochemical staining of mScarb2 protein. Scarb2 protein expression was observed in neurons in the spinal cord of $Scarb2^{+/+}$ mice (F) but not in the $Scarb2^{-/-}$ mice (G). Typical neurons expressing high levels of mScarb2 (stained brown) were indicated by arrowheads. Scarb2 protein expression was also observed in all muscle fibers of $Scarb2^{+/+}$ (H) but not in the $Scarb2^{-/-}$ mice (I). The scale bars indicate 50 μm.

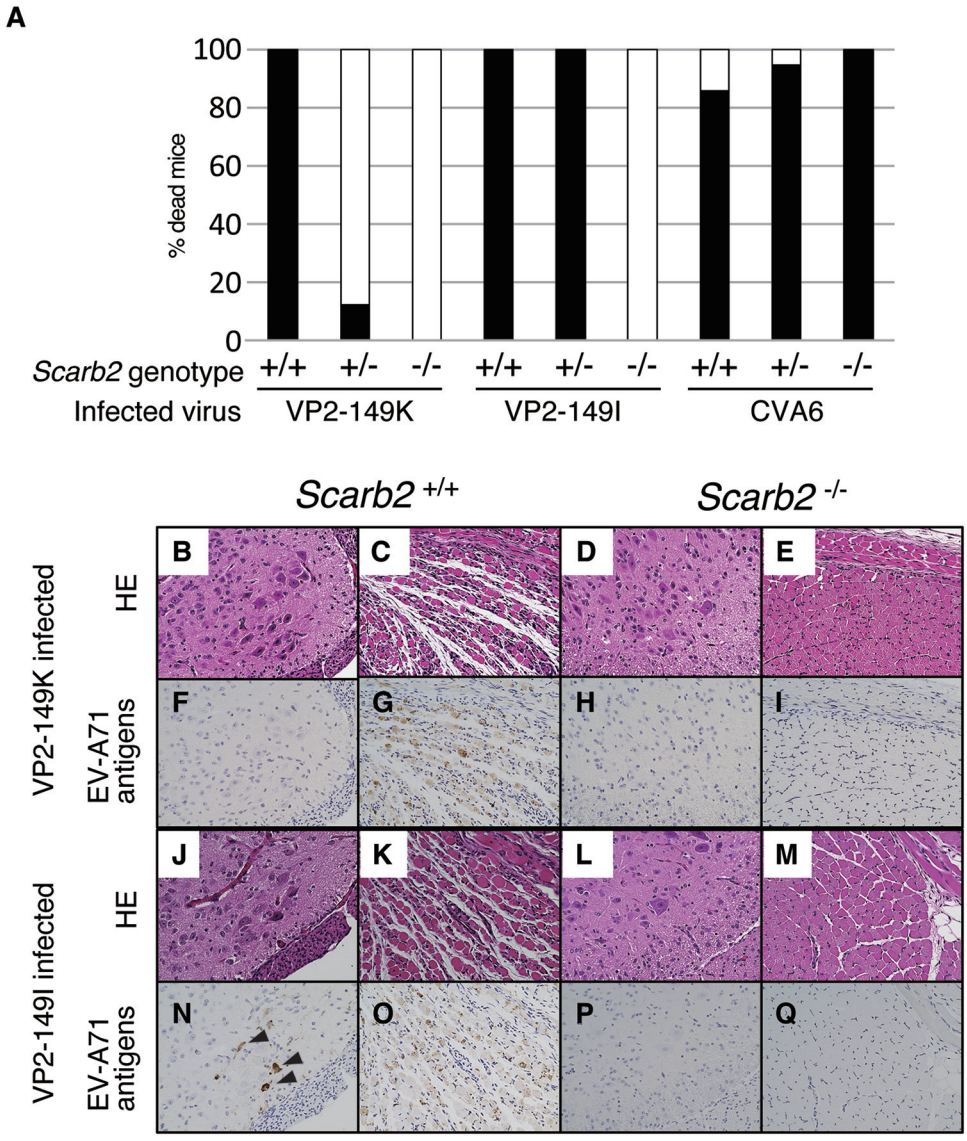

FIG 4 Scarb2 genotype and susceptibility. (A) Mortality of the mice of different *Scarb2* genotypes after infection with VP2-149K and VP2-149I strains. Stacked graph showing the proportion of dead mice (black) and surviving mice without clinical signs (white). (B to Q) Hematoxylin and eosin (H&E) and anti-EV-A71 antibody staining of EV-A71-infected mice. *Scarb2*$^{+/+}$ mice and *Scarb2*$^{-/-}$ mice were infected with the VP2-149K strain (top two rows) or VP2-149I strain (bottom two rows). The first and third rows from the top were stained with H&E, and the second and fourth rows were stained with EV-A71 antibody. Spinal cord (B, D, F, H, J, L, N, and P) and skeletal muscle (C, E, G, I, K, M, O, and Q) are shown. Note that EV-A71 antigens were positive in many muscle fibers infected with VP2-149K (G) and VP2-149I (O) and some neurons infected with VP2-149I indicated by arrowheads (N) in *Scarb2*$^{+/+}$ mice.

for each virus infection group were analyzed successfully. The relationship between genotype and mortality is shown in Fig. 4A. All *Scarb2*$^{+/+}$ mice (10 dead mice/10 infected mice) and 12% of *Scarb2*$^{+/-}$ mice (3/25) infected with the VP2-149K strain died. All *Scarb2*$^{+/+}$ (18/18) and *Scarb2*$^{+/-}$ (14/14) mice infected with the VP2-149I strain also died. In contrast, none of the *Scarb2*$^{-/-}$ mice infected with either strain died (0/8 and 0/9, respectively). In addition, no lesions or viral antigens were observed in the surviving *Scarb2*$^{-/-}$ mice (Fig. 4D, E, H, I, L, M, P, and Q; Table 1). In the CVA6 control group, almost all mice died irrespective of the *Scarb2* genotype (Fig. 4A). These results showed that the mice are susceptible to EV-A71 only when they have the WT *Scarb2* allele and that the *Scarb2*$^{-/-}$ mice are resistant to infection. Thus, it is clear that the infection of neonatal mice with WT (VP2-149K) and MA (VP2-149I) strains is mediated by mScarb2.

TABLE 1 Histopathological examination of mice infected with VP2-149K and VP2-149I strains

Virus	*Scarb2* genotype	No. of viral antigens in:			No. of lesions in:		
		Brain	Spinal cord	Muscle	Brain	Spinal cord	Muscle
VP2-149K	+/+	0/5[a]	1/5	5/5	0/5[b]	0/5	5/5
	+/−	0/5	0/5	2/5	0/5	0/5	2/5
	−/−	0/5	0/5	0/5	0/5	0/5	0/5
VP2-149I	+/+	5/5	5/5	5/5	0/5	0/5	5/5
	+/−	3/5	5/5	5/5	1/5	2/5	5/5
	−/−	0/5	0/5	0/5	0/5	0/5	0/5

[a]No. of mice antigen positive/no. of mice examined.
[b]No. of mice lesion positive/no. of mice examined.

Spread of infection and severity of disease are modulated by virus-receptor affinity. Previous studies showed that MA strains are more virulent than WT strains (15), but the reason for this difference in virulence has been unclear. Thus, we examined *Scarb2*$^{+/+}$ mice that died after infection with either VP2-149K or VP2-149I. Histopathological examination on five of the dead *Scarb2*$^{+/+}$ mice infected with each strain showed massive tissue destruction, inflammatory reactions, and EV-A71 antigens in the skeletal muscle and tongue of all VP2-149K-infected mice but only rarely were (one out of five) pathological lesions and viral antigens seen in the CNS (Fig. 4B, C, F, and G; Table 1). In contrast, viral antigens were detected not only in the skeletal muscle but also in neurons in the spinal cord, brainstem, midbrain, and hippocampus in all VP2-149I-infected mice (Fig. 4J, K, N, and O; Table 1). Taken together, the different strains produced different tropism phenotypes, with the WT strain showing muscle-tropic infection and the MA strains showing both muscle- and neurotropic infection. The difference in virulence between the VP2-149K and VP2-149I strains was also observed in *Scarb2*$^{+/-}$ mice. The mortality rate of VP2-149K-infected mice was 12%, while that of VP2-149I was 100% (Fig. 4A). In WT ICR neonatal mice of 0 to 2 weeks old infected intraperitoneally with 1.7×10^5 $TCID_{50}$ of either VP2-149K or VP2-149I, mortality was higher after VP2-149I infection than that after VP2-149K infection, irrespective of the age of the mice (Fig. 5A and B). Viral antigens were observed mainly in the muscle of VP2-149K-infected mice, whereas they were detected in both muscle and neurons of VP2-149I-infected mice (data not shown). These results suggested that the virus with higher infection efficiency spread more easily, had broader tropism, and exhibited a more virulent phenotype.

EV-A71 pathogenicity is altered by *Scarb2* expression levels. We next compared the outcomes of VP2-149K infection in *Scarb2*$^{+/+}$ and *Scarb2*$^{+/-}$ mice. *Scarb2*$^{+/+}$ mice showed 2-fold higher Scarb2 expression than *Scarb2*$^{+/-}$ mice and higher mortality (Fig. 3D and E). All of the *Scarb2*$^{+/+}$mice died, whereas only 12% of the *Scarb2*$^{+/-}$ mice died (Fig. 4A). The result indicated that the severity of disease in neonatal mice infected with VP2-149K is dependent on the expression level of mScarb2. In contrast to infection with VP2-149K, all *Scarb2*$^{+/+}$ *and Scarb2*$^{+/-}$ mice infected with the VP2-149I strain died. The results suggested that the expression level of Scarb2 is an important factor influencing the susceptibility of muscle to EV-A71 infection, especially when the VP2-149K strain is used.

Progressive loss of susceptibility with aging is associated with a decrease in *Scarb2* expression. The previous results led us to postulate that the age-associated susceptibility change of mice to EV-A71 infection might be influenced by Scarb2 expression. We examined the changes in susceptibility and mScarb2 expression using WT ICR neonatal mice. Most 0-week-old mice infected with the VP2-149K strain died (mortality, 81.8% [18/22]), whereas the mortality of 1-week-old mice infected with the VP2-149K strain was 29.2% (7/24). All mice older than 2 weeks of age survived without clinical signs (Fig. 5A). Similarly, all 0- and 1-week-old mice infected with VP2-149I died (Fig. 5B). All 2-week-old mice survived, but 50% of them showed clinical signs, such as weak paralysis and wobbling. All 3-week-old and older mice survived without clinical signs. The period of susceptibility to WT strain infection was shorter than that of the MA strains and that 2 and 3 weeks after birth are critical points for the loss of susceptibility, respectively.

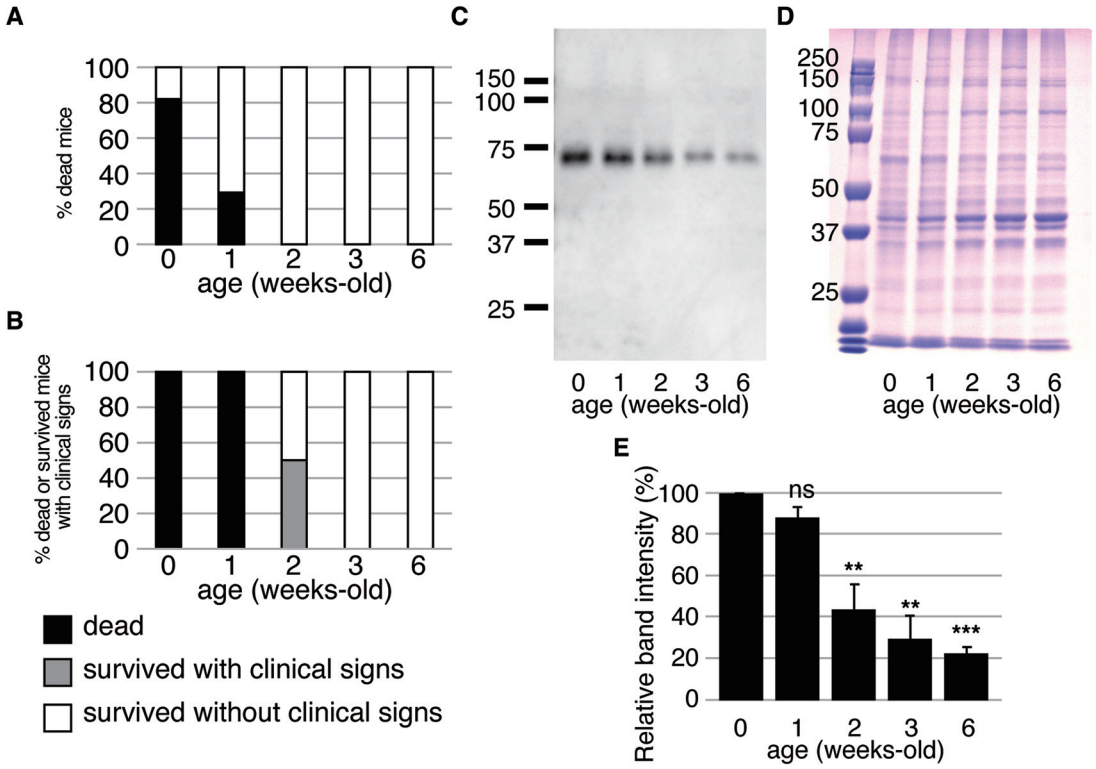

FIG 5 Age-associated decrease in susceptibility and Scarb2 expression. (A and B) The susceptibility of mice at different ages. The neonatal mice at 0 week (3 days), 1 week (9 days), 2 weeks (15 days), and 3 weeks (22 days) and adult (6 weeks) mice were infected intraperitoneally with 1.7×10^5 $TCID_{50}$ of VP2-149K (A) or VP2-149I (B) strains. The stacked graphs show the proportion of dead mice (black) and surviving mice with clinical signs (gray) or surviving without clinical signs (white). (C) Expression of Scarb2 in the muscle of different ages. The muscles from mice with above-indicated ages were isolated. Each lane was loaded with 130 ng of protein, and the blots were subjected to Western blotting using anti-mScarb2. (D) Coomassie brilliant blue staining of the same samples in B (4 μg/lane) as a loading control. (E) Relative amount of Scarb2 expression during development. The Scarb2 expression level was measured by densitometry, and Scarb2 expression in 0-week-old mice was set as 100%. The experiments were repeated three times, and the mean value $\pm$ standard deviation is shown. The statistical significance of the difference in values for each condition, using 0 weeks old as the standard, was determined by Student's *t* test and corrected by the Bonferroni method. ns, $P > 0.05$; **, $P < 0.01$; ***, $P < 0.001$.

Western blot analysis to determine Scarb2 expression levels showed that Scarb2 expression was high in the muscles of 0-week-old mice and then decreased progressively with aging (Fig. 5C to E). At 2 weeks after birth, the Scarb2 expression level was approximately half of that in 0-week-old mice, and in 3-week-old and older mice, the expression level was 30% of that in 0-week-old mice. When these expression patterns are compared with the difference in susceptibility of *Scarb2*$^{+/+}$ mice and *Scarb2*$^{+/-}$ mice to infection (Fig. 3D and E and Fig. 4A), it appears that a reduction in Scarb2 expression of 50% leads to a significant reduction in susceptibility to WT viruses. Thus, it is likely that the decrease in Scarb2 expression during development plays a role in the loss of susceptibility in neonatal mice.

The VP2-149 mutation does not affect the virulence of EV-A71 in hSCARB2 tg mice. VP2-149I and VP2-149M mutant strains are virulent in neonatal mice (17, 18), but it is unknown whether these mutants are virulent in humans. Thus, we examined the outcomes of infection with these strains in hSCARB2 tg mice, in which EV-A71 infection is mediated by hSCARB2 (12, 29, 30). A group of 10 6-week-old hSCARB2 tg mice were infected with the VP2-149K or VP2-149I strain, with doses ranging from 10^3 to 10^6 $TCID_{50}$. The mortality of mice infected with VP2-149K or VP2-149I was dose dependent, and the mortality rates at each dose were similar regardless of strain (Fig. 6A). We further defined the clinical scores of infected mice to compare the virulence of the two strains. There was no significant difference in clinical scores between the VP2-149K- and VP2-149I-infected groups at any inoculum dose (Fig. 6B). Viral antigens were detected in neurons in the brain stem and spinal cord of paralyzed mice, and the

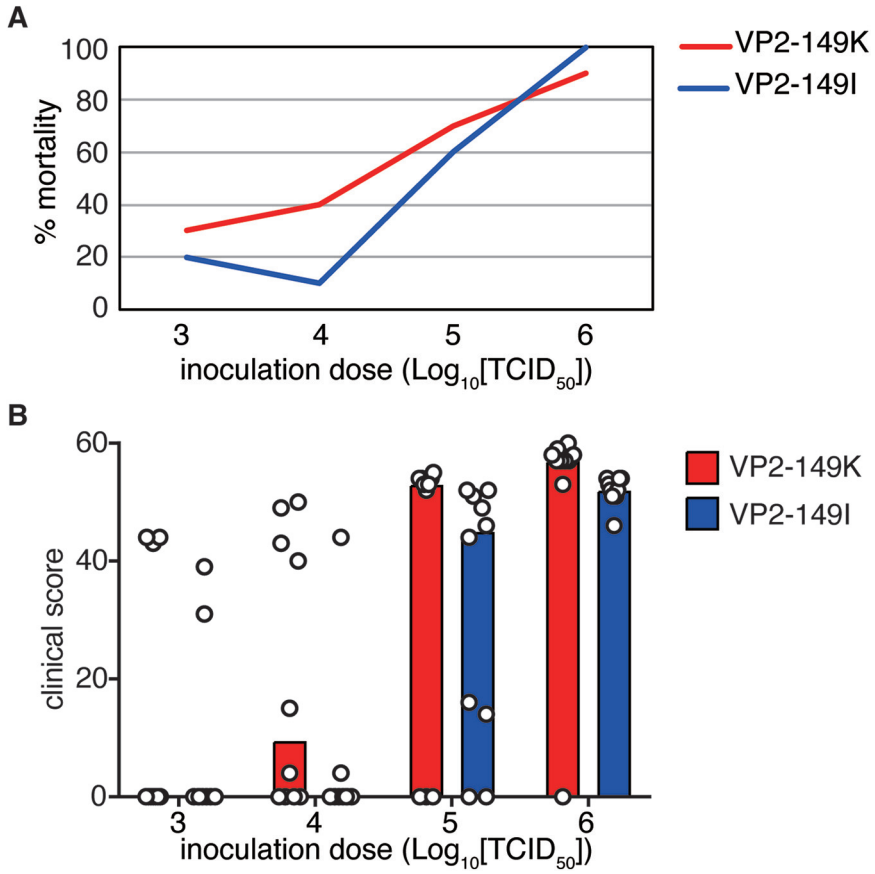

FIG 6 Mortality of hSCARB2 tg mice after infection with VP2-149K and VP2-149I strains. (A) hSCARB2 tg mice (10 per group) were infected intravenously with different strains and concentrations of virus as indicated. Mortality was monitored for 2 weeks. (B) Comparison of the clinical scores of the mice infected with VP2-149K and VP2-149I strains. The clinical score of each mouse was shown with circles, and the mean value of the infection group was shown as bars. No statistically significant differences were detected between the VP2-149K- and VP2-149I-infected groups for each dose by two-way ANOVA and Sidak's multiple-comparison test ($P > 0.1$).

distributions of the viral antigens and pathological lesions were similar between the two strains (data not shown). These results suggested that the virulence of the two strains in hSCARB2 tg mice is comparable and the MA (VP2-149I) strain has a more virulent phenotype only in neonatal mice due to the adaptation to mScarb2.

DISCUSSION

The mechanisms via which the host range, tissue tropism, and severity of EV-A71 disease are determined have remained unclear. WT EV-A71 cannot infect mouse L929 cells, although these cells express mScarb2, but it can infect L929 cells ectopically expressing hSCARB2 (9, 11, 13). Therefore, it was thought that mScarb2 does not have receptor activity. In this study, we have shown that both VP2-149K and VP2-149I strains of EV-A71 can use the mScarb2 protein as a receptor; however, the efficiency of infection via mScarb2 was very low for WT strains but not for the MA strains (Fig. 2). We further showed that infection with WT and MA strains was abolished in mice lacking a functional *Scarb2* gene (Fig. 4A). It is now clear that even WT strains of EV-A71 can use mScarb2 as a receptor *in vitro* and *in vivo*, albeit with low efficiency. The ambiguity in determining the host range of EV-A71 can be explained rationally by our experimental results. The interaction between WT EV-A71 and hSCARB2 is strong enough to establish infection in humans *in vivo* and *in vitro*. In contrast, the interaction between WT EV-A71 and mScarb2 is weak and borderline for successful infection. The establishment of infection, the spread of the virus, and severity of the disease can vary depending on

a number of factors, as discussed below. The results of this study do not appear to be consistent with those of previous studies using L929 that mScarb2 does not serve as receptor (9, 11, 13). This difference may be because L929 cells have lower permissiveness than RD cells, which in turn is probably due to the intrinsic antivirus response in L929 cells. We think that RD+hS2 and RD+mS2 cells are better systems to address this issue.

Scarb2 expression is observed in all organs (12). Skeletal muscle and neurons of the CNS, which are the main replication sites of EV-A71 in neonatal mice, do not express particularly higher levels of Scarb2 than nontarget tissues (Fig. 3F and H). This finding indicates that the tropism of viral infection is not determined by Scarb2 alone and that the reason why EV-A71 shows muscle-tropic infection in neonatal mice cannot be simply attributed to receptor expression. The MA mutation, which enhances the virus-receptor interaction, alters the mode of infection in mice. The main replication site of the WT strain is muscle; however, the MA strain infected both the CNS and the muscle (Fig. 4B to Q). We propose that the high-affinity interaction between the MA strain and mScarb2 facilitates the spread of infection from muscle to the CNS, resulting in the development of the virulent phenotype. Conversely, the efficiency of infection of VP2-149K and VP2-149I viruses via hSCARB2 is similar (Fig. 2B), and therefore, the two viruses did not show any significant difference in tropism and virulence in hSCARB2 tg mice (Fig. 6). These results suggest that apparent tropism and severity of the disease are modulated by the difference in infection efficiency.

The *Scarb2*$^{+/+}$ mice showed more severe disease than *Scarb2*$^{+/-}$ mice (in which mScarb2 expression is 50% lower than in *Scarb2*$^{+/+}$) when they were infected with the VP2-149K strain (Fig. 4A), indicating that mScarb2 expression levels affect virus pathogenicity. This finding might also explain the progressive loss of viral susceptibility with aging because the expression level of Scarb2 decreased gradually with aging. At 2 weeks of age, Scarb2 levels were 50% lower than that at 0 weeks old (Fig. 5C to E), and this result was associated with reduced susceptibility to the WT strain. Furthermore, at 3 weeks of age, when the expression level of mScarb2 was 30% of that at 0 weeks old, the susceptibility to MA strains was lost. The negative effect of reduced expression levels of Scarb2 on viral susceptibility was more pronounced with the WT strain than the MA strain (Fig. 5). It is likely that the decrease in Scarb2 expression with aging strongly influences viral susceptibility in mice. SCARB2 is required for the normal biogenesis and maintenance of lysosomes and endosomes and has been identified as the sorting receptor for β-glucocerebrosidase (31). Disruption of this gene results in action myoclonus-renal failure syndrome in humans (32, 33) and ureteric pelvic junction obstruction, deafness, and peripheral neuropathy in mice (34). Scarb2 expression, which must be regulated to maintain normal physiological functions, has been found to be controlled developmentally to decrease in skeletal muscle during the first few weeks of life in mice. We can coincidentally use mice as an EV-A71 infection model only when Scarb2 expression level is high. However, this decrease may not be the only reason for the age-associated decrease in susceptibility. Previous studies have shown that AG129 mice exhibit more severe disease and have a longer susceptibility period than WT mice (22), suggesting that IFN signaling induced by the maturation of innate immune response also plays an important role. It is therefore possible that both the decrease in Scarb2 expression and maturation of the innate immune response contribute to the progressive decrease in susceptibility with aging. Consistent with this idea, AG129 mice as old as 10 weeks of age were still susceptible to EV-71 when a MA strain was used (23). This result is probably because the high infection efficiency of the MA strain compensates for the low levels of mScarb2 expression, facilitating the infection of adult AG129 mice. We propose that the age-associated reduction Scarb2 expression is one of the reasons for the loss of susceptibility, in addition to maturation of innate immunity.

In this study, we have shown that EV-A71infection in neonatal mice is mediated by mScarb2. This interaction is weak and borderline for infection. Therefore, establishment of infection in mice is modulated by slight changes in virus-receptor affinity and the expression levels of the receptor in tissues during the developmental

stage. The host defense system may also modulate infection. All of these factors shape the pathology and severity of the disease. Differences in pathogenicity between the natural host and artificial animal models can be explained by the statuses of these factors in each host.

MATERIALS AND METHODS

Ethics statements. All experiments using recombinant DNA and pathogens were approved by the Committee for Experiments using Recombinant DNA and Pathogens at the Tokyo Metropolitan Institute of Medical Science (approval numbers 18-033, 19-009, and 20-003). All animal experiments were approved by the Animal Use and Care Committee (approval numbers 20-008, 20-070, and 21-024) and performed following the Guidelines for the Care and Use of Animals (Tokyo Metropolitan Institute of Medical Science, 2011). Mice exhibiting severe paralysis in more than two limbs or losing more than 30% of their body weight during the infection experiments were sacrificed using an overdose of isoflurane or by cervical dislocation.

Cells and viruses. Human rhabdomyosarcoma (RD-A) cells were provided from Hiroyuki Shimizu, National Institute of Infectious Diseases, Japan, and maintained in Dulbecco's modified Eagle's medium (DMEM) containing 5% fetal calf serum (FCS). RDΔS2 cells were established previously (25). The retrovirus vector plasmid (pQCIXP-hSCARB2-F) that expresses hSCARB2 with a FLAG tag was prepared as described previously (25). Mouse Scarb2 cDNA (13) was amplified using primers 5′-TCCGCGGCCGCACC GGTACCATGGGCCGATGCTGCTT-3′ and 5′-TCCGCGGCCGCGGTTCGAATGAGGGGTG-3′ using PrimeSTAR GXL DNA polymerase (TaKaRa). A retrovirus vector plasmid harboring mScarb2 (pQCIXP-mScarb2-F) was constructed by replacing the hSCARB2 cDNA sequence of pQCIXP-hSCARB2-F (NotI-NotI fragment) with the corresponding mScarb2 cDNA. The recombinant retrovirus was produced by transfecting pQCXIP-hSCARB2-F or pQCXIP-mScarb2-F together with pVSV-G (Clontech) into GP2-293 cells (Clontech). RDΔS2 cells were infected with the recombinant retroviruses. The cells expressing hSCARB2 (RD+hS2) and mScarb2 (RD+mS2) were selected in DMEM containing 5% FCS and 1 μg/mL puromycin. These cells were maintained in the same medium, and puromycin was omitted when they were used in the infection experiments.

Two cDNA fragments were amplified from the EV-A71 capsid region (position 1 to 1406 and 1388 to 1930) using PrimeSTAR GXL DNA polymerase, primers containing the VP2-149I mutation (NotI-T7-SK-EV-5 22, 5′-CGGCGGCCGCGTAATACGACTCACTATAGGTTAAAACAGCCTGTGGGTTG-3′, and VP2-149I-R, 5′-TGAGTCTG GATGTAAGGGGGGTGA-3′; or VP2-149I-F, 5′-CCCCTTACATCCAGACTCAACCCG-3′, and Ise1930-R, 5′-CCGG GAAGCGCAGCCTCTCC-3′), and pSVA-EV71-Isehara (25) as a template. The underline indicates the mutated codon (K to I). The amplified fragments were fused by PCR using primers NotI-T7-SK-EV-5 22 and Ise1930-R. The resulting fragment was digested with NotI and XhoI and cloned into the NotI-XhoI sites of pSVA-EV71-Isehara (pSVA-EV71-Isehara VP2-149I). pSVA-EV71-Isehara and pSVA-EV71-Isehara VP2-149I were digested with SalI and used as the template for *in vitro* transcription. Full-length RNAs of VP2-149K and VP2-149I strains were produced using the MEGAscript T7 transcription kit (Thermo Fisher Scientific). The viruses were recovered by transfecting the RNAs into RD-ΔEXT1+hSCARB2 cells (35) and propagated once.

Virus titer was determined by either microplate titration using RD-A cells or plaque assay on RD+hS2 and RD+mS2 cells, as described previously (25). The genome copy number of the virus was determined as described previously (35). Briefly, viral RNA was extracted using the QIAamp viral RNA minikit (Qiagen) followed by reverse transcription using PrimeScript RT master mix (TaKaRa). Quantitative PCR was conducted using enterovirus universal primer pairs (36), Thunderbird SYBR qPCR mix (Toyobo), and the StepOnePlus real-time PCR system (Applied Biosystems/Thermo Fisher Scientific).

Mice. Pregnant ICR mice were purchased from SLC Japan. Neonatal mice with the indicated ages were used for infection experiments. Human SCARB2 tg mice [C57BL/6 Tg(hSCARB2)10] (12) were maintained in a specific-pathogen-free facility. Six- to 7-week-old mice were used for infection experiments.

Generation of knockout mouse strains. The Scarb2 knockout mouse strain was generated using the CRISPR-Cas9 system (37–39). Scarb2 single guide RNA (sgRNA) was designed to target the sequence 5′-CACAAACAACTTCTGCTGAT(AGG)-3′, where the protospacer-adjacent motif (PAM) is indicated by the sequence in parentheses. To generate the DNA template for *in vitro* transcription, PCR amplification was performed using a forward primer containing the T7 promoter and target sequences (5′-CTTAAGCT AATACGACTCACTATAGGCACAAACAACTTCTGCTGATGTTTTAGAGCTAGAAATAGCAAGT-3′), reverse primer (5′-AAAAGCACCGACTCGGTGCC-3′), and synthetic gene of the sgRNA sequence (40) as a template. sgRNA was generated using the MEGAshortscript T7 transcription kit (Thermo Fisher Scientific) and purified using the MEGAclear transcription clean-up kit (Thermo Fisher Scientific) according to the manufacturer's instructions. The Cas9 protein and sgRNA were introduced into embryos using the electroporation method (41). All surviving embryos were transferred into the oviducts of pseudopregnant female mice.

***Scarb2* genotyping of mice.** A small piece of tail was cut and lysed in 10 mM Tris-HCl, 50 mM KCl, 1.5 mM $MgCl_2$, 0.45% Nonidet P-40, 0.45% Tween 20, 0.1% gelatin, and 0.5 mg/mL proteinase K at 55°C for 2 h, and then the proteinase K was inactivated at 95°C for 20 min. A knockout allele and WT alleles of *Scarb2* gene were detected by allele-specific PCR of genomic DNA of the mice using TaKaRa *Ex Taq* hot start version (TaKaRa) and primers WT-F (5′-ACTGGTTGGATTTTCTGTTTAGTC-3′) and WT-R (5′-GTGA ATCACAAACAACTTCTGCTG-3′) for the WT allele, and KO-F (5′-CCATGCTGAAAGCCTATCCAG-3′) and KO-R (5′-AGGCAATTTTGGTCTTCGCC-3′) for the *Scarb2* knockout allele. The thermal cycle was 94°C for 5 min, and then 35 cycles of 94°C for 15 sec, 60°C for 20 sec, and 72°C for 30 sec. The WT and knockout allele-specific primers produce 253- and 215-bp fragments, respectively.

Infection experiments. For the analysis of the pathogenicity of the Isehara VP2-149K and VP2-149I strains, 50 μL of Isehara VP2-149K or VP2-149I (1.7×10^5 $TCID_{50}$) was inoculated intraperitoneally into mice of 0 to 6 weeks old, and the survival was monitored for 2 weeks. Mortality in each age group was scored. Histological lesions and viral antigens were examined.

The correlation between the *Scarb2* genotype and susceptibility to infection was examined by inoculating the neonatal progeny of mated male and female *Scarb2*$^{+/-}$ mice within 3 days of birth with either the EV-A71 Isehara VP2-149K or the VP2-149I strain (1.7×10^5 $TCID_{50}$) or with the CVA6 1421-Yamagata-2008 strain (21 $TCID_{50}$) and observing the mice over a period of 10 days. The tails of the dead and surviving mice were isolated and subjected to genotyping. The hind limbs of the dead mice were removed, homogenized in approximately 10 volumes of DMEM containing 5% FCS, and centrifuged at 10,000 $\times$ *g* for 20 min. The presence of the virus was confirmed by inoculating the RD+hSCARB2 cells with the supernatants of the homogenates. Mice that died unexpectedly early (day 1 or 2 postinfection) and from which no replicating virus was detected in their hind limbs were determined to have died accidentally and were excluded from the analysis. The relationship between genotype and mortality was analyzed. The five *Scarb2*$^{+/+}$mice that died after VP2-149K infection, the *Scarb2*$^{+/+}$mice that died after VP2-149I infection, the *Scarb2*$^{+/-}$ and *Scarb2*$^{-/-}$ mice that survived VP2-149K infection, and the *Scarb2*$^{-/-}$ mice that survived VP2-149I infection were subjected to hematoxylin-eosin staining and detection of viral antigens.

For virulence analysis in hSCARB2 tg mice, 6-week-old hSCARB2 mice (10 mice per group) were inoculated intravenously with 200 μL of virus (10^3 to 10^6 $TCID_{50}$) and monitored for paralysis and survival for 2 weeks. The clinical score (0, no clinical signs; 1, wobbling; 2, difficulty in moving limbs [incomplete paralysis]; 3, complete flaccid paralysis of a limb or limbs; 4, moribund; 5, dead) of each mouse was recorded daily and summed over the observation period. The moribund mice and mice showing paralysis in more than two limbs were euthanized according to humane endpoint criteria.

Western blotting. For the analysis of Scarb2 expression in cells, 10^6 cells (RD, RDΔS2, RD+hS2, RD+mS2 cells, or mouse embryonic fibroblasts (MEFs) prepared from an embryonic day 12.5 [E12.5] embryo of *Scarb2*$^{+/+}$, *Scarb2*$^{+/-}$, and *Scarb2*$^{-/-}$ mice) were lysed in 100 μL of radioimmunoprecipitation assay (RIPA) buffer (25 mM Tris [pH 7.5], 150 mM NaCl, 1% NP-40, 1% sodium deoxycholate, 0.1% sodium dodecyl sulfate [SDS], 1 mM ethylenediaminetetraacetic acid [EDTA], and protease inhibitor cocktail ([Roche]). For the analysis of Scarb2 expression in muscle, muscle from the hindlimbs of mice with the indicated ages was removed and homogenized in a 10-fold volume of RIPA buffer using a homogenizer (Cell destroyer PS2000; Bio Medical Science, Japan). Protein content was determined using the *Pierce* bicinchoninic acid (BCA) protein assay kit (Thermo Fisher Scientific). A total of 200 ng (MEF samples) or 130 ng (muscle samples) of solubilized proteins were denatured in SDS sample buffer (Bio-Rad) at 70°C for 10 min, subjected to SDS-polyacrylamide gel electrophoresis, and transferred to polyvinylidene fluoride membranes. Proteins were detected using a goat anti-human LIMP-II/SR-B2 polyclonal antibody (AF1966; R&D Systems), a rabbit anti-mouse LIMP-II/SR-B2 monoclonal antibody (MAB1888: R&D Systems), a mouse anti-FLAG antibody conjugated with horseradish peroxidase (F7425; Sigma-Aldrich), or an anti-β-actin antibody conjugated with horseradish peroxidase (AC74; Sigma-Aldrich). The expression levels of the Scarb2 protein in MEF cells were compared after normalization by dividing the signal of Scarb2 antibody by that of β-actin antibody. For the muscle samples, the same samples were electrophoresed on a separate gel and stained by Coomassie brilliant blue as a loading control. The intensity of Scarb2 signals in Western blot were compared directly. The experiment was repeated three times to test for statistical significance.

Flow cytometry. RD, RD+hS2, and RD+mS2 cells (10^6) were detached using phosphate-buffered saline (PBS) containing 0.02% EDTA and incubated with goat anti-human LIMP-II/SR-B2 polyclonal antibody (1:33 dilution) for 1 h, washed with PBS twice, incubated with donkey anti-goat IgG H&L conjugated with Alexa Fluor 647 (1:33 dilution; ab150131; Abcam) on ice in the presence of propidium iodide (PI; 1:100 dilution), and analyzed on a FACSCanto II flow cytometer (BD Biosciences).

Immunohistochemistry. Dead mice were fixed in 4% paraformaldehyde in PBS. Paralyzed mice were euthanized by inhalation of high concentrations of isoflurane until respiratory arrest was confirmed. They were then fixed with 4% paraformaldehyde and the organs were removed. Organs were immersed in 50% ethanol (three changes, each immersion lasting for 3 days) to remove fat and in PBS containing 0.22 M EDTA and 71.3 mM citric acid monohydrate (three changes, each immersion lasting for 3 days) for decalcification and then embedded in paraffin. Thin sections of 4-μm thickness were prepared, deparaffinized, and stained with hematoxylin-eosin according to standard procedures. Virus antigens were detected using anti-EV-A71 rabbit polyclonal antibody, as described previously (12).

Statistical analyses. Student's *t*-tests were performed (Fig. 2B, 3E, and 5E). In multiple-comparison tests, *P* values were adjusted by the Bonferroni method (Fig. 2B). Two-way analysis of variance (ANOVA) and Sidak's multiple-comparison test were performed (Fig. 6B).

Data availability. Nucleotide sequence data for EV-A71 SI/Isehara/Japan/99, N772-Sendai-2006, 2716-Yamagata-2003, Y90-3896, and CVA6 1421-Yamagata-2013 strains are available in GenBank under accession numbers LC375764.1, LC506513.1, LC375766.1, LC506514.1, and LC421628.1, respectively.

ACKNOWLEDGMENTS

We thank Hidekazu Nishimura (Sendai virus center) and Katsumi Mizuta (Yamagata Prefectural Institute of Public Health) for providing EV-A71 and CVA6 virus strains and Naoki Kajiwara (Tokyo Metropolitan Institute of Medical Science) for fluorescence-activated cell sorting (FACS) analysis.

This work was supported in part by JSPS KAKENHI (grant number 19K07601 for K.K. and 18H026667 for S.K.) and by AMED (grant number 21fk0108084h1203 for S.K.).

REFERENCES

1. Racaniello V. 2013. Picornaviridae: the viruses and their replication, p 453–489. *In* Knipe D, Howley PM (ed), Fields virology, 6th ed. Wolters Kluwer Health/Lippincott Williams & Wilkins, Philadelphia, PA.
2. Pallansch M, Oberste MS, Whitton JL. 2013. Enteroviruses: polioviruses, Coxackieviruses, Echoviruses, and Newer Enteroviruses., p 490–530. *In* Knipe D, Howley PM (ed), Fields virology, 6th ed. Wolters Kluwer Health/Lippincott Williams & Wilkins, Philadelphia, PA.
3. WHO. 2011. A guide to clinical management and public health response for hand, foot and mouth disease (HFMD). https://apps.who.int/iris/handle/10665/207490.
4. Huang CC, Liu CC, Chang YC, Chen CY, Wang ST, Yeh TF. 1999. Neurologic complications in children with enterovirus 71 infection. N Engl J Med 341:936–942. https://doi.org/10.1056/NEJM199909233411302.
5. Chang LY, Huang YC, Lin TY. 1998. Fulminant neurogenic pulmonary oedema with hand, foot, and mouth disease. Lancet 352:367–368. https://doi.org/10.1016/S0140-6736(98)24031-1.
6. Puenpa J, Wanlapakorn N, Vongpunsawad S, Poovorawan Y. 2019. The history of Enterovirus A71 outbreaks and molecular epidemiology in the Asia-Pacific region. J Biomed Sci 26:75. https://doi.org/10.1186/s12929-019-0573-2.
7. He Y, Ong KC, Gao Z, Zhao X, Anderson VM, McNutt MA, Wong KT, Lu M. 2014. Tonsillar crypt epithelium is an important extra-central nervous system site for viral replication in EV71 encephalomyelitis. Am J Pathol 184:714–720. https://doi.org/10.1016/j.ajpath.2013.11.009.
8. Ooi MH, Solomon T, Podin Y, Mohan A, Akin W, Yusuf MA, del Sel S, Kontol KM, Lai BF, Clear D, Chieng CH, Blake E, Perera D, Wong SC, Cardosa J. 2007. Evaluation of different clinical sample types in diagnosis of human enterovirus 71-associated hand-foot-and-mouth disease. J Clin Microbiol 45:1858–1866. https://doi.org/10.1128/JCM.01394-06.
9. Yamayoshi S, Yamashita Y, Li J, Hanagata N, Minowa T, Takemura T, Koike S. 2009. Scavenger receptor B2 is a cellular receptor for enterovirus 71. Nat Med 15:798–801. https://doi.org/10.1038/nm.1992.
10. Yamayoshi S, Iizuka S, Yamashita T, Minagawa H, Mizuta K, Okamoto M, Nishimura H, Sanjoh K, Katsushima N, Itagaki T, Nagai Y, Fujii K, Koike S. 2012. Human SCARB2-dependent infection by coxsackievirus A7, A14, and A16 and enterovirus 71. J Virol 86:5686–5696. https://doi.org/10.1128/JVI.00020-12.
11. Yamayoshi S, Ohka S, Fujii K, Koike S. 2013. Functional comparison of SCARB2 and PSGL1 as receptors for enterovirus 71. J Virol 87:3335–3347. https://doi.org/10.1128/JVI.02070-12.
12. Fujii K, Nagata N, Sato Y, Ong KC, Wong KT, Yamayoshi S, Shimanuki M, Shitara H, Taya C, Koike S. 2013. Transgenic mouse model for the study of enterovirus 71 neuropathogenesis. Proc Natl Acad Sci U S A 110:14753–14758. https://doi.org/10.1073/pnas.1217563110.
13. Yamayoshi S, Koike S. 2011. Identification of a human SCARB2 region that is important for enterovirus 71 binding and infection. J Virol 85:4937–4946. https://doi.org/10.1128/JVI.02358-10.
14. Zhou D, Zhao Y, Kotecha A, Fry EE, Kelly JT, Wang X, Rao Z, Rowlands DJ, Ren J, Stuart DI. 2019. Unexpected mode of engagement between enterovirus 71 and its receptor SCARB2. Nat Microbiol 4:414–419. https://doi.org/10.1038/s41564-018-0319-z.
15. Kobayashi K, Koike S. 2021. Adaptation and virulence of enterovirus-A71. Viruses 13:1661. https://doi.org/10.3390/v13081661.
16. Wang YF, Chou CT, Lei HY, Liu CC, Wang SM, Yan JJ, Su IJ, Wang JR, Yeh TM, Chen SH, Yu CK. 2004. A mouse-adapted enterovirus 71 strain causes neurological disease in mice after oral infection. J Virol 78:7916–7924. https://doi.org/10.1128/JVI.78.15.7916-7924.2004.
17. Chua BH, Phuektes P, Sanders SA, Nicholls PK, McMinn PC. 2008. The molecular basis of mouse adaptation by human enterovirus 71. J Gen Virol 89:1622–1632. https://doi.org/10.1099/vir.0.83676-0.
18. Huang SW, Wang YF, Yu CK, Su IJ, Wang JR. 2012. Mutations in VP2 and VP1 capsid proteins increase infectivity and mouse lethality of enterovirus 71 by virus binding and RNA accumulation enhancement. Virology 422:132–143. https://doi.org/10.1016/j.virol.2011.10.015.
19. Miyamura K, Nishimura Y, Abo M, Wakita T, Shimizu H. 2011. Adaptive mutations in the genomes of enterovirus 71 strains following infection of mouse cells expressing human P-selectin glycoprotein ligand-1. J Gen Virol 92:287–291. https://doi.org/10.1099/vir.0.022418-0.
20. Zaini Z, Phuektes P, McMinn P. 2012. A reverse genetic study of the adaptation of human enterovirus 71 to growth in Chinese hamster ovary cell cultures. Virus Res 165:151–156. https://doi.org/10.1016/j.virusres.2012.02.009.
21. Muller U, Steinhoff U, Reis LF, Hemmi S, Pavlovic J, Zinkernagel RM, Aguet M. 1994. Functional role of type I and type II interferons in antiviral defense. Science 264:1918–1921. https://doi.org/10.1126/science.8009221.
22. Khong WX, Yan B, Yeo H, Tan EL, Lee JJ, Ng JK, Chow VT, Alonso S. 2012. A non-mouse-adapted enterovirus 71 (EV71) strain exhibits neurotropism, causing neurological manifestations in a novel mouse model of EV71 infection. J Virol 86:2121–2131. https://doi.org/10.1128/JVI.06103-11.
23. Caine EA, Partidos CD, Santangelo JD, Osorio JE. 2013. Adaptation of enterovirus 71 to adult interferon deficient mice. PLoS One 8:e59501. https://doi.org/10.1371/journal.pone.0059501.
24. Ke X, Zhang Y, Liu Y, Miao Y, Zheng C, Luo D, Sun J, Hu Q, Xu Y, Wang H, Zheng Z. 2020. A single mutation in the VP1 gene of enterovirus 71 enhances viral binding to heparan sulfate and impairs viral pathogenicity in mice. Viruses 12:883. https://doi.org/10.3390/v12080883.
25. Kobayashi K, Sudaka Y, Takashino A, Imura A, Fujii K, Koike S. 2018. Amino acid variation at VP1-145 of enterovirus 71 determines attachment receptor usage and neurovirulence in human scavenger receptor B2 transgenic mice. J Virol 92:e00681-18. https://doi.org/10.1128/JVI.00681-18.
26. Imura A, Sudaka Y, Takashino A, Tamura K, Kobayashi K, Nagata N, Nishimura H, Mizuta K, Koike S. 2020. Development of an enterovirus 71 vaccine efficacy test using human scavenger receptor B2 transgenic mice. J Virol 94:e01921-19. https://doi.org/10.1128/JVI.01921-19.
27. Mizuta K, Tanaka S, Komabayashi K, Aoki Y, Itagaki T, Katsushima F, Katsushima Y, Yoshida H, Ito S, Matsuzaki Y, Ikeda T. 2019. Phylogenetic and antigenic analyses of coxsackievirus A6 isolates in Yamagata, Japan between 2001 and 2017. Vaccine 37:1109–1117. https://doi.org/10.1016/j.vaccine.2018.12.065.
28. Staring J, van den Hengel LG, Raaben M, Blomen VA, Carette JE, Brummelkamp TR. 2018. KREMEN1 is a host entry receptor for a major group of enteroviruses. Cell Host Microbe 23:636–643.e5. https://doi.org/10.1016/j.chom.2018.03.019.
29. Chu ST, Kobayashi K, Bi X, Ishizaki A, Tran TT, Phung TTB, Pham CTT, Nguyen LV, Ta TA, Khu DTK, Agoh M, Pham AN, Koike S, Ichimura H. 2020. Newly emerged enterovirus-A71 C4 sublineage may be more virulent than B5 in the 2015-2016 hand-foot-and-mouth disease outbreak in northern Vietnam. Sci Rep 10:159. https://doi.org/10.1038/s41598-019-56703-5.
30. Kobayashi K, Nishimura H, Mizuta K, Nishizawa T, Chu ST, Ichimura H, Koike S. 2021. Virulence of enterovirus A71 fluctuates depending on the phylogenetic clade formed in the epidemic year and epidemic region. J Virol 95:e0151521. https://doi.org/10.1128/JVI.01515-21.
31. Gonzalez A, Valeiras M, Sidransky E, Tayebi N. 2014. Lysosomal integral membrane protein-2: a new player in lysosome-related pathology. Mol Genet Metab 111:84–91. https://doi.org/10.1016/j.ymgme.2013.12.005.
32. Blanz J, Groth J, Zachos C, Wehling C, Saftig P, Schwake M. 2010. Disease-causing mutations within the lysosomal integral membrane protein type 2 (LIMP-2) reveal the nature of binding to its ligand beta-glucocerebrosidase. Hum Mol Genet 19:563–572. https://doi.org/10.1093/hmg/ddp523.
33. Hopfner F, Schormair B, Knauf F, Berthele A, Tolle TR, Baron R, Maier C, Treede RD, Binder A, Sommer C, Maihofner C, Kunz W, Zimprich F, Heemann U, Pfeufer A, Nabauer M, Kaab S, Nowak B, Gieger C, Lichtner P, Trenkwalder C, Oexle K, Winkelmann J. 2011. Novel SCARB2 mutation in action myoclonus-renal failure syndrome and evaluation of SCARB2 mutations in isolated AMRF features. BMC Neurol 11:134. https://doi.org/10.1186/1471-2377-11-134.
34. Gamp AC, Tanaka Y, Lullmann-Rauch R, Wittke D, D'Hooge R, De Deyn PP, Moser T, Maier H, Hartmann D, Reiss K, Illert AL, von Figura K, Saftig P. 2003. LIMP-2/LGP85 deficiency causes ureteric pelvic junction obstruction, deafness and peripheral neuropathy in mice. Hum Mol Genet 12:631–646. https://doi.org/10.1093/hmg/ddg062.
35. Kobayashi K, Mizuta K, Koike S. 2020. Heparan sulfate attachment receptor is a major selection factor for attenuated enterovirus 71 mutants during cell culture adaptation. PLoS Pathog 16:e1008428. https://doi.org/10.1371/journal.ppat.1008428.
36. Jonsson N, Gullberg M, Israelsson S, Lindberg AM. 2009. A rapid and efficient method for studies of virus interaction at the host cell surface using

enteroviruses and real-time PCR. Virol J 6:217. https://doi.org/10.1186/1743-422X-6-217.
37. Wang H, Yang H, Shivalila CS, Dawlaty MM, Cheng AW, Zhang F, Jaenisch R. 2013. One-step generation of mice carrying mutations in multiple genes by CRISPR/Cas-mediated genome engineering. Cell 153:910–918. https://doi.org/10.1016/j.cell.2013.04.025.
38. Yang H, Wang H, Shivalila CS, Cheng AW, Shi L, Jaenisch R. 2013. One-step generation of mice carrying reporter and conditional alleles by CRISPR/Cas-mediated genome engineering. Cell 154:1370–1379. https://doi.org/10.1016/j.cell.2013.08.022.
39. Aida T, Chiyo K, Usami T, Ishikubo H, Imahashi R, Wada Y, Tanaka KF, Sakuma T, Yamamoto T, Tanaka K. 2015. Cloning-free CRISPR/Cas system facilitates functional cassette knock-in in mice. Genome Biol 16:87. https://doi.org/10.1186/s13059-015-0653-x.
40. Hwang WY, Fu Y, Reyon D, Maeder ML, Tsai SQ, Sander JD, Peterson RT, Yeh JR, Joung JK. 2013. Efficient genome editing in zebrafish using a CRISPR-Cas system. Nat Biotechnol 31:227–229. https://doi.org/10.1038/nbt.2501.
41. Kaneko T, Sakuma T, Yamamoto T, Mashimo T. 2014. Simple knockout by electroporation of engineered endonucleases into intact rat embryos. Sci Rep 4:6382. https://doi.org/10.1038/srep06382.